the plant journal

SEB SOCIETY FOR EXPERIMENTAL BIOLOGY

The Plant Journal (2022) **109,** 664–674 doi: 10.1111/tpj.15585

Sponging of glutamate at the outer plasma membrane surface reveals roles for glutamate in development

Vanessa Castro-Rodríguez[1], Thomas J. Kleist[1], Nicoline M. Gappel[1], Fatiha Atanjaoui[1], Sakiko Okumoto[2], Mackenzie Machado[3], Tom Denyer[4], Marja C. P. Timmermans[4], Wolf B. Frommer[1,5] and Michael M. Wudick[1]*

[1]*Institute for Molecular Physiology, Heinrich-Heine-Universität Düsseldorf, Düsseldorf, Germany,*
[2]*Department of Soil and Crop Science, Texas A&M, College Station, TX, USA,*
[3]*Department of Plant Biology, Carnegie Institution for Science, Stanford, CA, USA,*
[4]*Center for Plant Molecular Biology, University of Tübingen, Auf der Morgenstelle 32, Tübingen 72076, Germany, and*
[5]*Institute of Transformative Bio-Molecules (WPI-ITbM), Nagoya University, Chikusa, Nagoya 464-8601, Japan*

Received 1 May 2020; revised 3 November 2021; accepted 8 November 2021; published online 16 November 2021.
*For correspondence (e-mail wudick@hhu.de).

SUMMARY

Plants use electrical and chemical signals for systemic communication. Herbivory, for instance, appears to trigger local apoplasmic glutamate accumulation, systemic electrical signals, and calcium waves that travel to report insect damage to neighboring leaves and initiate defense. To monitor extra- and intracellular glutamate concentrations in plants, we generated Arabidopsis lines expressing genetically encoded fluorescent glutamate sensors. In contrast to cytosolically localized sensors, extracellularly displayed variants inhibited plant growth and proper development. Phenotypic analyses of high-affinity display sensor lines revealed that root meristem development, particularly the quiescent center, number of lateral roots, vegetative growth, and floral architecture were impacted. Notably, the severity of the phenotypes was positively correlated with the affinity of the display sensors, intimating that their ability to sequester glutamate at the surface of the plasma membrane was responsible for the defects. Root growth defects were suppressed by supplementing culture media with low levels of glutamate. Together, the data indicate that sequestration of glutamate at the cell surface either disrupts the supply of glutamate to meristematic cells and/or impairs localized glutamatergic signaling important for developmental processes.

Keywords: ***Arabidopsis thaliana*, glutamate, root meristem, fluorescence, biosensor.**

INTRODUCTION

As a building block of proteins and central player in metabolism, glutamate is an essential amino acid for all known forms of life. In addition, many organisms also utilize L-glutamate as a signaling molecule. Glutamatergic signaling has been most intensively studied in the context of the animal central nervous system, where it serves as an excitatory neurotransmitter through activation of metabotropic and ionotropic glutamate receptors. In plants, glutamate is essential for the assimilation of nitrogen and for transamination (Forde and Lea, 2007). Low amounts of externally supplied glutamate are known to affect root architecture by impairing primary root growth while favoring the development of secondary roots (Walch-Liu et al., 2006). Various lines of evidence implicate glutamate itself as a signaling molecule also in plants. For instance, mutants with lesions in *GLUTAMATE RECEPTOR-LIKE* (*GLR*) ion channel genes, encoding proteins for which glutamate can act as an agonist, show altered wound responses as a consequence of impaired propagation of wound-induced variation potentials (Mousavi et al., 2013; Nguyen et al., 2018). Notably, it has been shown that external application of glutamate to leaves elicits long-distance, calcium-based plant defense responses (Toyota et al., 2018).

Genetically encoded biosensors that rely on changes in Förster resonance energy transfer (FRET) efficiency of two fluorescent proteins (FPs) have been engineered and used to dynamically report levels of several metabolites and signaling molecules in living cells (Frommer et al., 2009; Okumoto et al., 2012). By sandwiching a bacterial periplasmic binding protein (YbeJ) between enhanced cyan FP (ECFP) and Venus, a yellow FP (YFP) variant (Okumoto et al., 2005), we engineered the first FRET-based fluorescent indicator proteins for glutamate (FLIPE). Subsequent systematic modification of first-generation glutamate sensors yielded a series of optimized sensors with varying ligand affinities and dynamic ranges (Deuschle et al., 2005).

However, the optimized variants could not be used in neuronal cells, as they did not traffic efficiently to the cell surface (Okumoto unpublished). Subsequently, the intensiometric single-fluorophore iGluSnFRs were engineered by insertion of a circularly permutated green FP (GFP) into YbeJ (Marvin et al., 2013). Toyota et al., (2018) successfully targeted iGluSnFR to the apoplasmic space to estimate glutamate concentrations after wounding of Arabidopsis (*Arabidopsis thaliana*) leaves (Toyota et al., 2018). Because circularly permutated GFP-based sensors are particularly sensitive to pH changes, the use of ratiometric FRET-based sensors is advantageous for *in vivo* imaging (Barnett et al., 2017). We therefore sought to deploy a suite of ratiometric FLIPE variants spanning a wide range of affinities to enable monitoring extra- and intracellular levels of glutamate in Arabidopsis.

Plants expressing cytosolic versions of FLIPE showed wild-type-like growth phenotypes. Unexpectedly, when FLIPEs were anchored in the plasma membrane and displayed extracellularly, transformants were severely stunted and showed defects in root and flower development, as well as growth. The severity of the phenotype depended on the affinity of the sensors, and symptoms could be ameliorated by supplementation with glutamate, consistent with a model wherein surface-displayed sensors interfere with glutamate availability close to the plasma membrane, thereby disrupting growth and development.

RESULTS

Expression of extracellularly displayed FLIPEs causes stunting and lethality

With the intent of generating plants for quantitative imaging of glutamate dynamics, a suite of FLIPE affinity variants with dissociation constants ranging from nanomolar to millimolar concentrations of glutamate was introduced into Arabidopsis and either targeted to the cytosol (FLIPE^{cyt}) or tethered to the extracellular face of the plasma membrane, which we refer to here as "display" sensors (FLIPE^{display}). FLIPE^{display} and FLIPE^{cyt} cassettes were constructed by sandwiching the *Escherichia coli* periplasmic glutamate binding protein YbeJ between two spectral variants of the GFP. Cell surface display was achieved by fusion of an endoplasmic reticulum (ER) targeting sequence to the N-terminus of the chimera and the mammalian platelet-derived growth factor receptor (PDGFR) transmembrane spanning domain to its C-terminus (Figure S1). The sensors were expressed under control of the ubiquitous CaMV 35S promoter in *rdr6-11* gene silencing mutants (Deuschle et al., 2006) and visually selected for fluorescence (Figure S2a). For lines expressing the extracellularly displayed FLIPE, we noticed a positive correlation between the sensor dissociation constant (K_d) and severe growth defects (Figure 1a). Among soil-grown plants, rosette sizes of plants expressing extracellularly displayed sensors with affinities of 600 nM–100 μM were significantly smaller, with rosette areas 20–50% of the *rdr6-11* controls (Figure 1b). Moreover, plants expressing the FLIPE-100μ^{display} and FLIPE-1m^{display} were the only transgenic lines that generated seeds, albeit with reduced frequencies for display versions (9–32%) relative to controls (99%) (Table 1). To test whether noxiousness depends on the affinity of the binding protein, new sensors with intermediate affinities (approximately 40 μM, FLIPE-40μ; approximately 250 μM, FLIPE-250μ; approximately 500 μM, FLIPE-500μ) were engineered by site-directed mutagenesis, and lines that display these sensors at the cell surface were generated and phenotyped (FLIPE-40μ^{display}, FLIPE-250μ^{display}, and FLIPE-500μ^{display}; Figure S1, Figure S3). The majority of the plants expressing display sensors with intermediate affinities were dwarfed. Plants expressing the wild-type YbeJ cassette (FLIPE-600n^{display}) were most affected (95%; Figure 1c). Intermediate affinity mutants showed "intermediate" (up to 34%) or wild-type (up to 15%) growth phenotypes (Figure 1c). The defects could be caused either by effects of the binding cassette at the surface of the plasma membrane, scavenging glutamate in the apoplasmic space, or by processes in the secretory system. To evaluate if secretory system effects play a role, or if surface display, rather than mere apoplasmic localization of the sensors, was a prerequisite for the defects, a secreted version of FLIPE-600n carrying only the ER targeting sequence but lacking the PDGFR transmembrane domain was engineered (FLIPE-600n^{apo}; Figure S1). Different from the displayed FLIPE-600n version, the majority of FLIPE-600n^{apo}-expressing plants showed wild-type-like growth (87%), similar to plants expressing the cytosolic FLIPE version of the same affinity (FLIPE-600n^{cyt}; Figure 1c, Figure S4a,b). As both display and apoplasmic sensors have to pass through the secretory system, the noxious effects are likely due to extracellular glutamate scavenging. Moreover, the presence of the sensor in the apoplasmic space did not seem to cause defects, whereas tethering to the extracellular face of the plasma membrane was likely causative for the observed developmental and growth defects. Specifically, we hypothesize that display of high-affinity glutamate-binding FLIPEs at the surface of the plasma membrane affects glutamate levels in the vicinity of receptors or transporters that are important for proper growth and development.

No differences in fluorescence intensities were observed among plants expressing the full range of displayed FLIPE affinity variants (Figure S2a), indicating that sensor noxiousness was not caused by differences in expression levels. To exclude possible effects of the position of the fusion of the FPs on the noxiousness of the sensors, we generated and analyzed plants expressing high-affinity FLIPE sensors with altered sensor cassette topology, where ECFP was inserted into the YbeJ cassette at amino acid position 81 (FLII^{81}PE-1μ, Deuschle et al., 2005; FLII^{81}PE-10μ, Figure S1). While plants expressing the display version of the FLII^{81}PE-1μ

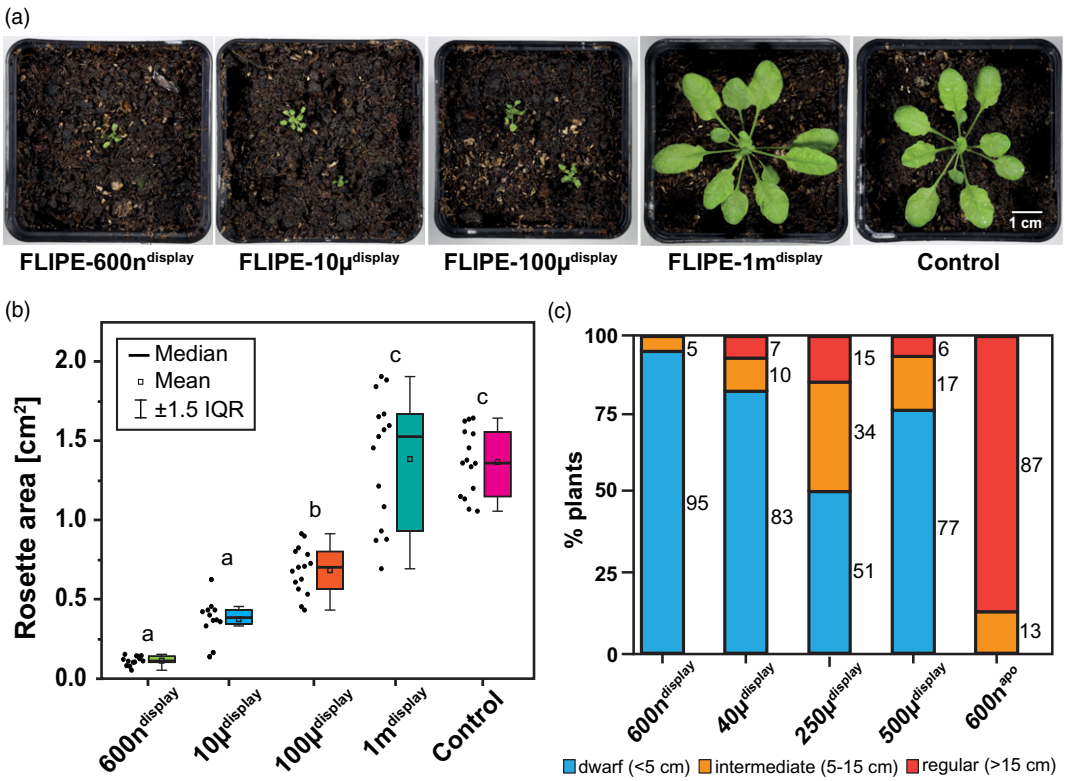

Figure 1. Phenotypic characterization of FLIPE sensor-expressing plants.
(a) Representative phenotypes of 6-week-old plants grown on soil under short-day conditions, expressing FLIPE sensor affinity variants and the corresponding *rdr6-11* control.
(b) Quantification of rosette areas of 3-week-old soil-grown plants expressing different FLIPE sensors ($n \geq 12$ plants per genotype from four independent biological replicates). Compared with *rdr6-11* control plants, FLIPE-600n^{display}, FLIPE-10µ^{display}, and FLIPE-100µ^{display} plants showed significantly smaller rosettes, respectively, while the rosette sizes of the cytosolic sensor variants and of the low-affinity FLIPE-1m^{display} line were not significantly different from the control (Tukey test, $P < 0.001$, letters indicate if samples are statistically indifferent [same letters] or different [different letters] from one another).
(c) Phenotypic characterization into "dwarf," "intermediate," and "regular" growth of several FLIPE^{display} and a FLIPE^{apo} version ($n \geq 21$).

Table 1 Effect of FLIPE sensor variants on the lethality in Arabidopsis grown under long day conditions

		No. of plants that survived after				
Sensor	No. of plants transferred to soil	Week 2	Week 4	Week 6	% Survival[a]	% Lethality[a]
FLIPE-600n^{display}	55	12	3	0	0	100
FLIPE-10µ^{display}	51	15	7	0	0	100
FLIPE-100µ^{display}	65	19	11	6	9	90
FLIPE-1m^{display}	73	34	30	23	32	68
FLII^{81}PE-1µ^{cyt}	107	106	106	106	99	1
FLII^{81}PE-10µ^{cyt}	109	108	108	108	99	1
Control (*rdr6-11*)	103	102	102	102	99	1

[a]Developmental stage: 6 weeks after germination, flowering, and forming seeds.

sensor phenocopied plants producing the high-affinity FLIPE sensors (K_d approximately 600 nM–100 µM), plants expressing cytosolically targeted versions of the FLII^{81}PE sensors (K_d approximately 1 µM, 10 µM), were statistically indistinguishable from controls (Figure S4c, Figure S5, Table 1). To exclude the possibility that noxiousness of high-affinity display sensors was caused by the membrane anchor, we replaced the PDGFR transmembrane domain with a polypeptide based on a previously described membrane anchor (Martinière et al., 2018), yielding FLIPE-600n^{display}-TM26 (Figure S1). Stable expression of the TM26-anchored FLIPE resulted in severely dwarfed plants, which were indistinguishable from plants expressing PDGFR-anchored sensors of the same affinity (Figure S4d),

providing further evidence for the hypothesis that membrane display is imperative for noxiousness.

To determine the subcellular localization of the FLIPEs carrying different targeting signals, spinning disk confocal microscopy was performed on roots of FLIPE-expressing plants. FLIPE sensors lacking targeting signals expectedly localized to the cytosol (Figure 2a,b, Figure S6). While the localization of the display sensors was mostly limited to the plasma membrane (Figure 2d–f, Figure S6), we occasionally also observed apparent ER localization. Localization in ER-like structures was also observed for the apoplasmic sensor as would be expected for heterologous proteins entering the secretory pathway. However, although FLIPE-600n^{apo} was present in internal membranes (likely representing the ER), noxiousness was not observed, excluding a role along the secretory pathway (Figure 1c, Figure S4e).

Surface display was evaluated in two ways, i.e., (i) by quantitative analysis of the sensor response, and by (ii) testing protease sensitivity. Consistent with the predicted surface display of the sensors, concentration-dependent changes in the fluorescence ratio were observed in response to perfusion of roots from FLIPE-10μ^{display}-expressing plants with a K_d of approximately 10 μM (similar to the K_d of the sensor; Figure S7). Protease sensitivity assays provided additional evidence for the surface display of FLIPE-1m^{display}. In contrast to the stable fluorescence from the cytosolic FLII^{81}PE-1μ^{cyt} sensor, which was unaffected by preincubation with the protein synthesis inhibitor (cycloheximide [CHX]), followed by proteinase K digestion in tobacco leaf protoplasts, fluorescence of FLIPE-1m^{display}-expressing protoplasts decreased by approximately one-third relative to protoplast treated with CHX alone (t = 42 min; Figure S8). These two sets of experiments support the display sensor topology wherein the ligand-binding domain of YbeJ faces the apoplasmic space and therefore is exposed to exogenously supplied protease.

Noxiousness might also be explained by differential proteolytic processing of cytosolic or apoplasmic sensors by

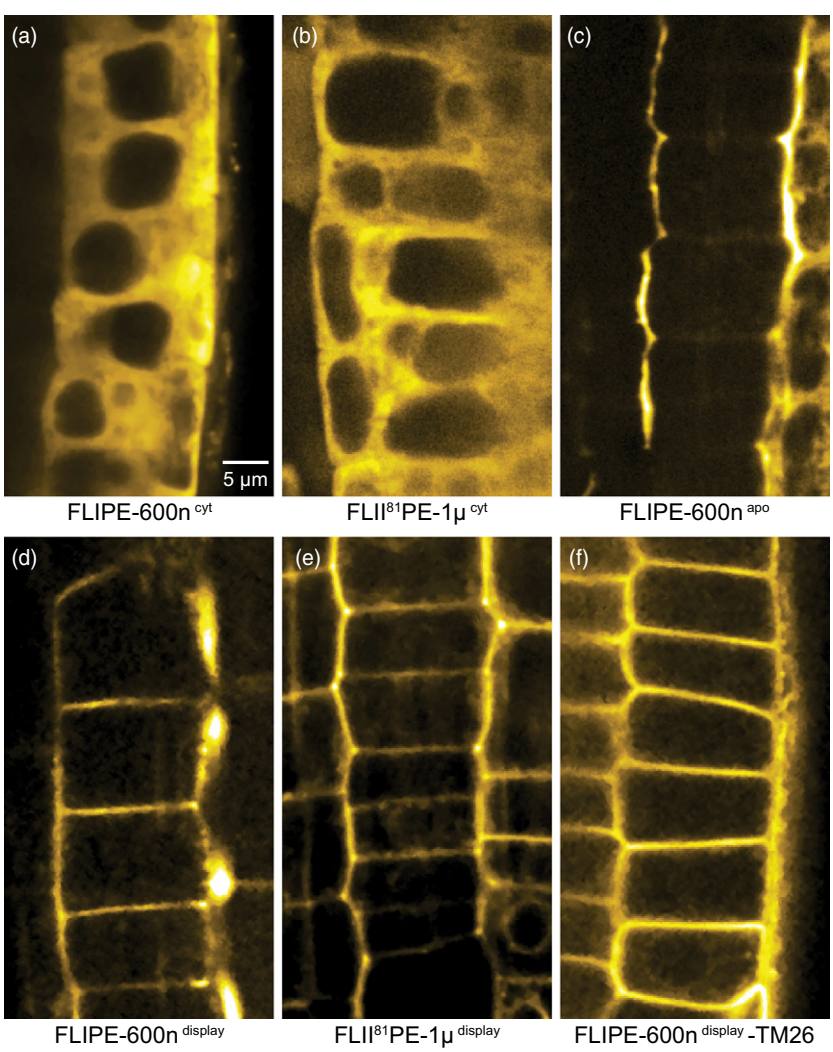

Figure 2. Subcellular localization of FLIPE sensors in the root proximal elongation zone.
Representative confocal images of 3–5-day-old plants expressing (a) FLIPE-600n^{cyt}, (b) FLII^{81}PE-1μ^{cyt}, (c) FLIPE-600n^{apo}, (d) FLIPE-600n^{display}, (e) FLII^{81}PE-1μ^{display}, or (f) FLIPE-600n^{display}-TM26 sensors. While sensors lacking additional targeting sequences accumulate throughout (a,b) the cytosol, (c) the apoplasmically expressed sensor showed an accumulation in the cell wall space and endoplasmic reticulum-like endomembranes, and (d–f) the display sensors were predominantly localized to the plasma membrane but could also be detected in endoplasmic reticulum-like structures. Excitation and exposure times were independently adjusted to allow qualitative comparisons.

endogenous proteases, i.e., by favoring cleavage of cytosolic variants. Indeed, in addition to polypeptides corresponding to the full-length versions of sensors targeted to the cytosol, plasma membrane, or apoplasm, protein gel blots also revealed fragments of lower apparent molecular masses migrating in similar patterns, albeit for all sensors regardless of their subcellular localization (Figure S9). We therefore infer those proteolytic events most likely cannot explain the lack of noxiousness in plants expressing the high-affinity sensor either in the cytosol or the apoplasm.

Developmental defects in FLIPE^{display} lines

Phenotypic analyses of FLIPE^{display}-expressing plants were performed to determine if the physiological effects of the FLIPE^{display} sensors impacted other aspects of plant development. Floral morphology was markedly different between FLIPE^{display} and control plants or cytosolic versions. Typically, flowers from dwarfed FLIPE^{display} plants were characterized by deformed or missing petals and failed to produce seeds (Figure 3). Morphological phenotypes were also observed and characterized in roots. Specifically, the root length of FLIPE^{display} lines showed an inverse proportionality to the affinity of the sensors for glutamate (i.e., plants expressing sensors with higher affinities for glutamate had shorter primary roots). As the extracellular glutamate concentration affects mitotic activity in the root apical meristem (RAM; Walch-Liu et al., 2006), RAMs from select FLIPE lines were examined. The majority of roots stably expressing the high-affinity FLIPE-600n^{display} sensor were severely deformed, likely due to aberrant growth and irregular cell divisions (Figure S10). Consequently, we were unable to unambiguously identify cell types and tissue layers in >80% of FLIPE-600n^{display}-expressing roots and therefore excluded them from further analyses. While plants expressing FLIPE-10μ^{display} and FLIPE-100μ^{display} sensors showed defective cell division patterns in the root meristem that affected the quiescent center (QC), columella, and root cap cells, none of the roots were as severely affected as the roots expressing the FLIPE-600n^{display} sensor (Figure 4, Figure S10). Five to six days after germination, the root tips of control seedlings typically consisted of five tiers of cells, one or two of which represent stem cell tiers while the remaining tiers of differentiated cells are characterized by an accumulation of starch granules (Kiss et al., 1996). We observed similar cellular patterns in RAMs of plants expressing FLII^{81}PE-1μ^{cyt}, FLII^{81}PE-10μ^{cyt}, and FLIPE-1m^{display} sensors as in *rdr6-11* controls (Figure 4, Figure S5e). Although roots from plants expressing FLIPE-10μ^{display} and FLIPE-100μ^{display} showed disorganized QC and columella cells, >50% of the mutants displayed at least one stem cell tier (Figure 4). Phenotypes of FLIPE^{display} plants are consistent with defects in the stem cell niche (affecting the overall number of cells), causing reduced root growth. As the above-ground tissues of plants expressing high-affinity FLIPE^{display} variants were severely dwarfed, it is possible that high-affinity FLIPE^{display} sensors also affect the development of the shoot meristem. Although not studied in detail here, together with the observed alterations in flower morphology, the findings tentatively point to a role for glutamate in developmental processes in meristems.

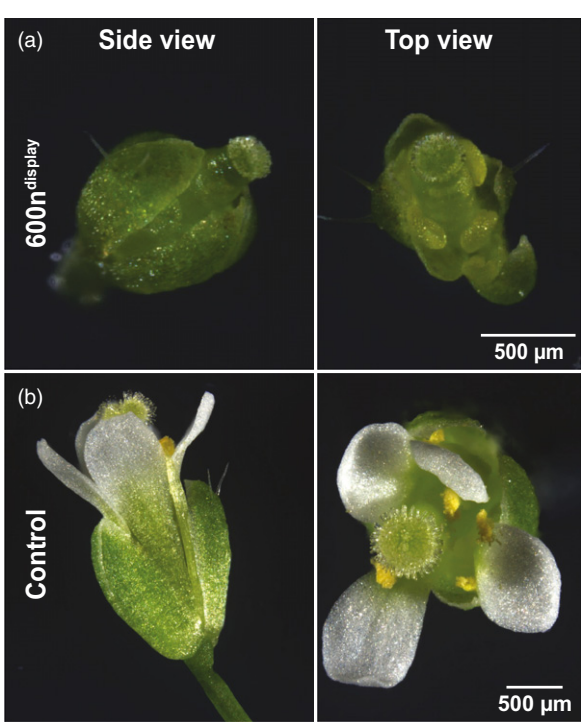

Figure 3. Phenotype of flowers from Arabidopsis control plants and lines expressing FLIPE- 600n^{display}.
Representative flowers from (a) FLIPE-600n^{display} or (b) control (*rdr6-11*) plants.

Glutamate supplementation mitigates root growth defects in FLIPE^{display} lines

The affinity-dependent effects of FLIPE^{display} lines indicate that the observed phenotypes may be caused by competitive binding (sponging) of extracellular glutamate at the cell surface. We therefore hypothesized that the growth defects could be suppressed by supplementing media with glutamate. Six-day-old seedlings expressing FLIPE-600n^{display} and untransformed controls were transferred from AM media to AM supplemented with glutamate. Exogenously supplied L-glutamate (eGlu) impairs primary root growth and increases the number of secondary roots (Walch-Liu et al., 2006). Accordingly, while low concentrations of eGlu (0–25 μM) had little to no observable effect on root length of *rdr6-11* control plants, higher eGlu concentrations (>100 μM) led to shorter primary roots (Figure 5a). In contrast, root lengths of FLIPE-600n^{display}-expressing plants grown on media with 25–1000 μM eGlu were roughly twice as long

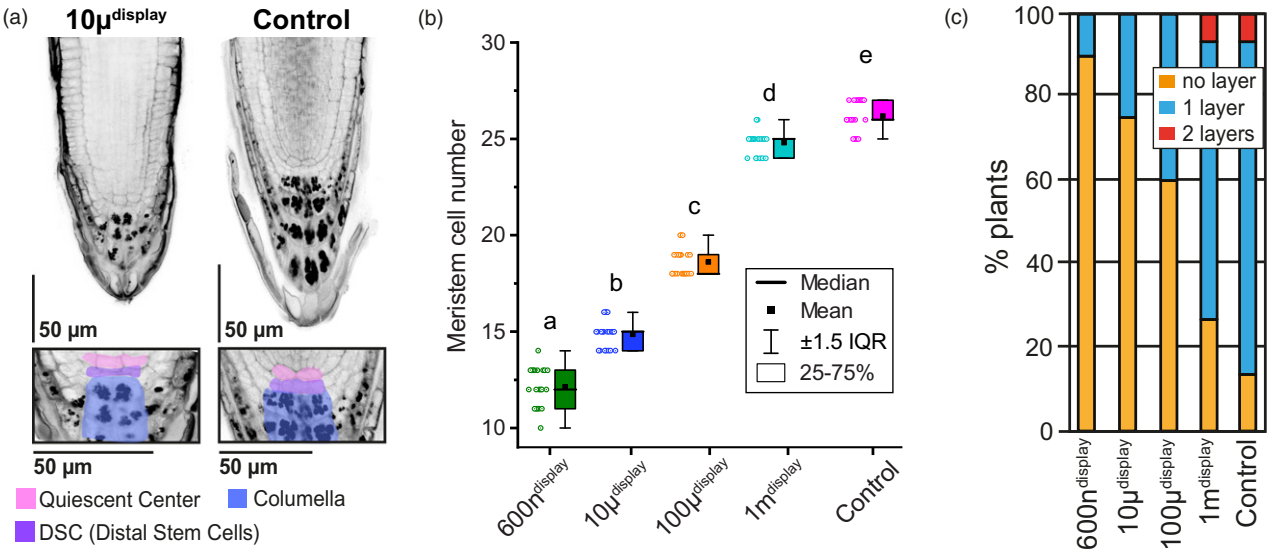

Figure 4. Effect of FLIPE sensor expression on the root apical meristem and the distal stem cell niche.
(a) Representative root tips of plants expressing display and cytosolic FLIPE variants grown on AM media for 3–5 days after germination (top panel) and zoom-in of respective proximal meristems (lower panel). The color code highlights the quiescent center (pink), distal stem cells (DSC, purple) and Columella cells (blue).
(b) Comparison of the size of the meristematic zone of the different FLIPE sensor lines, displaying the number of meristematic cells between the quiescent center and root elongation zone. Meristem cell numbers were statistically different in FLIPE-600n^{display}, FLIPE-10µ^{display}, and FLIPE-100µ^{display}, compared with the control (*rdr6-11*) (Tukey test $P < 0.001$, letters indicate if samples are statistically indifferent [same letters] or different [different letters] from one another). Data were acquired from six independent biological replicates, $n = 17–21$.
(c) Percentage of roots with no clearly identifiable or undifferentiated DSC layer (yellow bar), one cell layer (blue bar) or two cell layers (red bar); experiment performed three times independently with similar results; $n = 22$.

compared with controls grown without glutamate supplementation. Therefore, supplementation with eGlu appeared to suppress the dwarf phenotype of plants expressing FLIPE-600n^{display} sensors, at least partially. Even at eGlu concentrations that inhibited root growth in *rdr6-11* plants, FLIPE-600n^{display}-expressing plants showed increased primary root lengths compared with roots of plants grown in the absence of eGlu (Figure 5a). While glutamate concentrations >25 µM elicited a previously described increase in the number of lateral roots in *rdr6-11* control plants (Walch-Liu et al., 2006), FLIPE-600n^{display} plants did not show altered lateral root numbers (Figure 5b). Overall, eGlu treatment oppositely affected *rdr6-11* control and FLIPE-600n^{display}-expressing plants. Sponging of glutamate at the cell surface could cause the defects in the meristems of plants expressing high-affinity FLIPE^{display} constructs either by limiting the supply of glutamate to meristematic cells or by preventing effective glutamate signaling processes in these cells. To distinguish between these two hypotheses, we analyzed cell-type-specific levels of mRNAs associated with glutamate metabolism.

Transcripts of glutamate-associated genes are present in QC and surrounding cells

To profile the transcripts linked to glutamate-associated processes in the root tip meristem, single-cell RNA sequencing data from Arabidopsis root tips of 6-day-old seedlings clustered by cell type and developmental stage (Denyer et al., 2019) were analyzed. Plants are able to synthesize glutamate through distinct enzymatic pathways, i.e., involving genes for *GLUTAMINE-α-OXOGLUTARATE AMINOTRANSFERASE* (*GOGAT*), *GLUTAMINE SYNTHETASE* (*GS*), and *GLUTAMATE DEHYDROGENASE* (*GDH*) in the presence of a nitrogen source (Forde and Lea, 2007). Our analysis revealed that transcripts of three different *GS* isoforms (*GS1;1*, *GS1;3*, and *GS2*), as well as of *GOGAT2*, *GDH1*, and the ammonium transporter *AMT1.1* were indeed detected in the QC and/or in surrounding cell layers (Figure S11), intimating that these cells are capable of synthesizing glutamate *de novo*. While transcripts of genes expected to be downstream signaling targets of glutamate (i.e., members of the *GLUTAMATE RECEPTOR-LIKE* [*GLR*] family of ion channels) showed low levels and lacked specific expression patterns (not shown), transcripts of a putative *LYSINE/HISTIDINE TRANSPORTER* gene (*LHT4*) were enriched in QC and surrounding cells (Figure S11). Homologs of LHT4 had previously been shown to mediate glutamate transport in rice (*Os*LHT1) and Arabidopsis (*At*LHT1) (Hirner et al., 2006; Wang et al., 2019). Taken together, transcriptomic data imply that root meristematic cells should be capable of synthesizing glutamate from inorganic ammonium, prompting us to hypothesize that aberrant

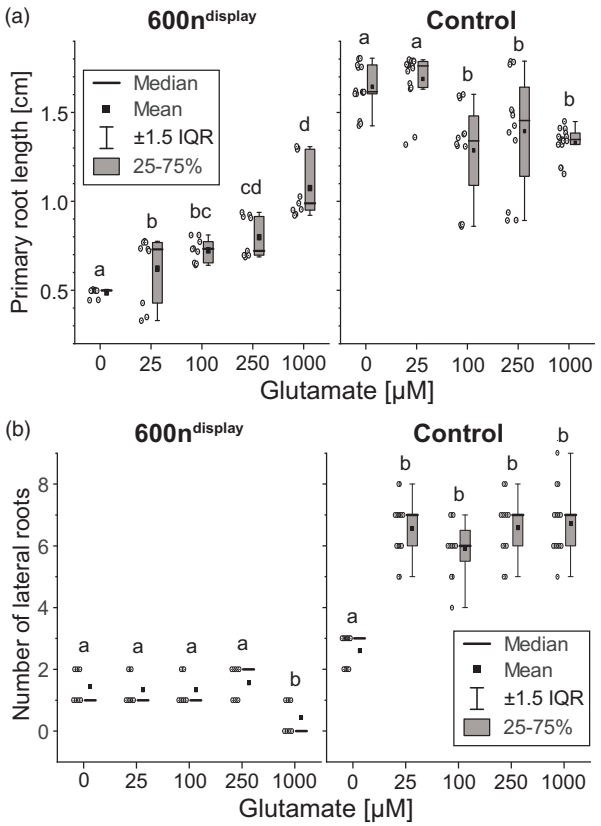

Figure 5. Supplementation with glutamate of FLIPE-600n^{display}-expressing plants.
(a) Primary root growth of vertically grown FLIPE-600n^{display} (left) or *rdr6-11* control (right) Arabidopsis seedlings 5 days after transfer to AM agar medium plates with increasing concentrations of glutamate. While roots of control plants did not significantly grow at [glu] ≥ 100 µM, roots lengths of FLIPE-600n^{display}-expressing lines increased even at the highest [glu] tested (1 mM).
(b) Number of lateral roots of FLIPE-600n^{display} (left) or *rdr6-11* control plants (right). Letters indicate if data were statistically indifferent (same letters) or different (different letters) from one another. Experiment was repeated three times independently with ≥3 roots per treatment yielding similar results.

glutamatergic signaling processes may underlie the observed noxiousness of FLIPE^{display} sensors. Together with the observations that only extracellularly displayed sensors caused developmental defects that could be partially alleviated by glutamate supplementation, we propose that sponging of eGlu directly at the outer face of the plasma membrane of meristematic cells has noxious effects on plant growth and development.

DISCUSSION

With the initial intent to monitor glutamate dynamics *in planta*, Arabidopsis lines stably expressing a suite of Arabidopsis lines expressing FLIPE in the cytosol and displayed at the cell surface were generated. Surprisingly, plants expressing high-affinity FLIPE display variants were severely dwarfed and showed reduced or no fertility. The severity of the phenotype correlated positively with the affinity of the sensors for glutamate (i.e., high-affinity variants caused the most dramatic phenotypes). Previous characterization of the YbeJ-binding domain revealed that it binds glutamate with an order of magnitude higher affinity than aspartate, and has substantially lower affinities for glutamine and asparagine (Okumoto et al., 2005; Willis and Furlong, 1975). We therefore hypothesized that the phenotypes were caused by depletion of the glutamate pool at the cell surface due to the glutamate-binding activity of FLIPE constructs. Correspondingly, two high-affinity constructs (FLIPE-600n, FLII^{81}PE-1µ) were only effective in causing developmental effects when anchored at the plasma membrane facing the apoplasm, while neither cytosolically nor apoplasmically targeted variants produced developmental or other phenotypic defects. Consistent with the hypothesis of glutamate depletion, supplementation of the media with extracellular glutamate partially restored growth in plants expressing extracellularly displayed, membrane-anchored high-affinity sensors. Sensor noxiousness could be due either to glutamate starvation in particular cell types, i.e., in the RAM, or to perturbed glutamatergic signaling. Starvation is an unlikely cause, otherwise one may have expected that apoplasmic sponging would have the same noxious effect as found in display lines. The observation that transcripts for several glutamate-related genes are present in root meristematic cells, appears at odds with the hypothesis that glutamate starvation underpins FLIPE noxiousness. Moreover, sequestration of glutamate either in the cell wall space or the cytosol (in plants expressing sensors targeted to the apoplasm or cytosol, respectively) would be expected to interfere with metabolism in a qualitatively similar manner to FLIPE^{display} expression. Another possible explanation for the difference between cytosolic and display sensor effects could be that one of them is preferentially degraded, thus preventing (or causing) noxious effectors. Proteolytic degradation patterns of differently targeted FLIPEs were comparable and therefore most likely cannot explain (lack of) noxiousness. The preferred hypothesis is thus that FLIPE sensors interfere with glutamatergic signaling at the membrane surface, presumably by local buffering of glutamate pools in the vicinity of GLRs that may interfere with downstream signaling processes. Sequestration or buffering by transgenes has been described in plants, e.g., in the case of a genetically encoded cAMP sponge (Sabetta et al., 2019) or a parvalbumin-derived calcium buffer (Huang et al., 2017).

For glutamate to function as a signaling molecule, it presumably must be kept at low resting levels in the extracellular space, particularly in the vicinity of glutamate receptors. In animals, this is well-established and achieved by the action of multiple sets of transporters in pre- and postsynaptic neurons, as well as adjacent glial cells

(Mahmoud et al., 2019). Interestingly, the effect of YbeJ-based glutamate indicators (iGluSnFR) on glutamate signaling in mice cortex astrocytes was recently studied. In a striking analogy to our findings, the authors come to the conclusion that extracellularly displayed sensors can act as glutamate buffers that reduce the extrasynaptic glutamate concentration, thereby slowing down glutamate uptake and yielding shorter synaptic transporter currents (Armbruster et al., 2020).

The main difference between plants and animals, however, is that the volume of the synaptic cleft is extremely small, thus requiring only small amounts of glutamate to be released and subsequently taken up again for desensitization, while the apoplasmic space between plant cells is many orders of magnitudes larger, suggesting a need for different mechanisms. Therefore, efficient glutamate uptake and redistribution mechanisms are particularly important in plants, which use glutamate as a major transport form of nitrogen. Indeed, while the concentrations of most amino acids in plants may change substantially during the diurnal cycle, glutamate in the leaf apoplasm appears to be homeostatic between 0.3 and 1.3 mM, depending on the species (Forde and Lea, 2007). GLRs have previously been implicated in meristem maintenance, developmental regulation, and glutamatergic signaling processes in roots (Li et al., 2006; Singh and Chang, 2017; Singh et al., 2016; Vincill et al., 2013). Similar to FLIPE^{display}-expressing plants, rice plants carrying mutations in *GLR3.1* displayed short roots with reduced QC cell numbers and an impaired cell division activity of the RAM (Li et al., 2006). Further evidence that glutamate-induced, GLR-mediated signaling is important for root development comes from the observation that glutamate receptor agonists negatively affected the primary root length and the number of secondary roots (Singh and Chang, 2017). The authors reported that, similar to the effects of glutamate resupply on FLIPE-expressing lines, exogenous application of glutamate was able to restore primary root growth as well as the number of lateral roots, further indicating that root development relies on glutamate signaling processes. A recent publication determined the apparent *in vitro* dissociation constant for glutamate of the GLR3.3 ligand-binding domain with K_d = 2.2 ± 0.5 μM (Alfieri et al., 2020). This value is very similar to the apparent affinities for glutamate of the FLIPE-600n and FLII^{81}PE-1μ constructs we used (with $K_d \approx$ 600 nM and 1 μM, respectively), and might support the idea of competitive binding of the glutamate by the FLIPE constructs.

Future studies should examine if the buffering of glutamate occurs in specific membrane (nano-) domains, as membrane compartmentalization and the establishment of functional sub-membrane domains were shown to be critical for plant cell signaling events (Chu et al., 2021; Gronnier et al., 2017).

The noxious effects of FLIPE^{display} sensors render them unsuitable for glutamate imaging, for instance during wounding. Analysis of glutamate dynamics are thus best performed with untethered apoplasmic glutamate sensors with appropriate affinities. Our study cautions that targeting of YbeJ-derived sensors might impact plant physiology. If able to be deployed inducibly, extracellularly displayed YbeJ chimeras may however provide a novel tool to study glutamatergic signaling in plants.

In summary, our data suggest that the level of glutamate specifically at the cell surface is important for glutamatergic signaling, thus requiring tight control via transport processes. Moreover, our data may support a role for glutamate in the regulation of developmental processes, in particular in root, shoot, and floral meristems.

EXPERIMENTAL PROCEDURES

FLIPE constructs for plant transformation

FLIPE surface display constructs carrying tandemly fused murine immunological kappa chain signal peptides, the YbeJ coding sequence (also called GltI; NP_415188, amino acid residues 29–302), and the transmembrane domain of the PDGFR were constructed as described previously (Okumoto et al., 2005). Except for the FLII^{81}PE constructs (see below), the YbeJ coding sequence was sandwiched between sequences encoding ECFP and Venus, an YFP. The resulting construct was excised using *Bam*HI/*Xho*I, and subcloned into *Bam*HI/*Sal*I sites of the plant expression vector CF203 (a pPZP212 derivative; Hajdukiewicz et al., 1994) containing the CaMV 35S-promoter, GFP5(S65T) gene and a rbcS terminator (kindly provided by C. Fankhauser, Lausanne). Affinity mutants were designed from wild-type YbeJ ($K_d \approx$ 600 nM) carrying different substitutions in position 179: A179R ($K_d \approx$ 10 μM), A179V ($K_d \approx$ 100 μM), and A179W ($K_d \approx$ 1 mM) (Okumoto et al., 2005) and additional intermediate affinities that were generated in this work: A179Q (K_d = 40 ± 0.87 μM; mean ± SEM n = 9), A179Y (K_d = 256 ± 4.63 μM; mean ± SEM n = 9) and A179N (K_d = 514 ± 8.92 μM; mean ± SEM n = 9). Fluorescent indicator proteins for glutamate (FLIPE) sensors were named FLIPE-x^{display} or FLIPE-x^{cyt} depending on their expression at the surface (display) or in the cytosol (cyt), respectively. The resulting plasmids were called: FLIPE-600n^{display}; FLIPE-10μ^{display}; FLIPE-40μ^{display}; FLIPE-100μ^{display}; FLIPE-250μ^{display}; FLIPE-500μ^{display}; FLIPE-1m^{display}; and FLIPE-600n^{cyt}. The FLIPE-600n^{display}-TM26 construct was generated using In-Fusion technology by replacing the PDGFR transmembrane domain with a previously described transmembrane domain (Martinière et al., 2018). In addition, a FLIPE-600n^{display}-based construct lacking the C-terminal PDGFR transmembrane domain was generated (FLIPE-600n^{apo}) for apoplasmic targeting. The cytosolic and display variants of the FLII^{81}PE-1μ and FLII^{81}PE-10μ sensor are based on a previously published construct (Deuschle et al., 2005), where the ECFP is inserted into the YbeJ cassette after amino acid 81, which was subsequently subcloned into the CF203 vector. Generated plasmids with complete sequence information will be made available via Addgene upon publication.

Agrobacterium tumefaciens GV3101 was transformed with the binary vectors and *A. thaliana rdr6-11* silencing mutants were transformed by floral dipping. Seeds were surface-sterilized with 70% ethanol for 5 min followed by 30% sodium hypochlorite for 10 min and rinsed with sterile, deionized water. Transformants

were selected on AM media (half-strength Murashige and Skoog basal salt mixture, including MES buffer (catalog no. M0254.0050; Duchefa Biochemie, Haarlem, The Netherlands) supplemented with 1% plant agar (pH 5.7) (catalog no. 9002-18-0; Sigma-Aldrich, Darmstadt, Germany) and 1% sucrose. Seedlings were grown vertically under long-day light conditions (16-h light, 8-h dark) at a light intensity of about 100 μmol m^{-2} sec^{-1} for 3 days. To identify plant expressing the sensor, seedlings were preliminarily screened for GFP fluorescence (bandpass excitation filter at λ_{ex} = 470/40 nm, bandpass emission filter at λ_{em} = 525/50 nm, with a beam splitter at λ_{em} = 495 nm) using a fluorescence stereo zoom microscope ZEISS Axio Zoom.V16, which can detect ECFP and Venus fluorescence. Plant transformation with FLIPE sensors was carried out independently at least three times and yielded comparable results.

In vitro characterization of FLIPE affinity variants

Affinity mutants carrying the substitution A179Q, A179Y, and A179N were created by site-directed mutagenesis, and cloned into pRSET vector for protein expression in *E. coli*, adding an N-terminal 6xHis-tag to the constructs. Sequences were verified by sequencing. pRSET-FLIPE constructs were transferred to *E. coli* BL21 (DE3) Gold (Stratagene, La Jolla, CA, USA) by chemical transformation. Colonies were inoculated in LB-media containing carbenicillin (catalog no. 4800-94-6; Sigma-Aldrich), 0.2% lactose (catalog no. 7660.0250; Merck) and 0.05% glucose (catalog no. 14431-43-7; Sigma-Aldrich) and expressed for 2 h at 37°C, shaking at 220 rpm, and then 48 h at 20°C in darkness. Cells were harvested by centrifugation for 30 min at 4°C and 13 000 *g*. Sediments were resuspended in 20 mM sodium phosphate buffer (pH 7.0) containing protease inhibitors and lysed by sonication (Branson Sonifier cell disruptor B15, Branson Ultrasonics, Brookfield, CT, USA; 10 cycles [15 sec ON/OFF]; 60% amplitude; 90% duty cycle), after which the lysate was centrifuged for 1 h at 4°C and 13 000 ***g***. Supernatants were purified by histidine-affinity chromatography. 6xHis-tagged proteins were eluted from the beads by using imidazole (catalog no. A1073,0500; UN3263; AppliChem, Darmstadt, Germany). Ligand titration curves were performed by using a microplate reader TECAN™ Spark®. ECFP fluorescence was acquired at λ_{ex} = 430/10 nm and λ_{em} = 470/10 nm, respectively. Venus fluorescence was recorded with a bandpass excitation filter at λ_{ex} = 500/10 nm and a bandpass emission filter at λ_{em} = 530/10 nm. Intensity scans were performed at λ_{ex} = 430/10 nm and λ_{em} = 460–600/10 nm. All analyses were done using 20 mM sodium phosphate buffer (pH 7.0). The K_d of each FLIPE variant was determined by fitting to a single site-binding isotherm, as described previously (Okumoto et al., 2005). Affinities were calculated from at least three independent protein extracts.

Plant growth

Transgenic *A. thaliana* (L.) Heynh. lines stably expressing display, cytosolic or apoplasmic FLIPE or FLII^{81}PE constructs were grown in soil Floradur® (Floragard Vertriebs-GmbH products, Oldenburg, Germany) in individual 2.5-inch pots. Pots were arrayed in a 4 × 8 grid in standard greenhouse flats (Hermann Meyer KG products, Willich, Germany) and transferred to growth chambers with short day (8 h light, 16 h dark) conditions at 21°C and 50–70% relative humidity, unless stated differently. Plants were watered as needed, depending on growth stage. To determine rosette sizes, plants were imaged every week during 5 weeks until flowering. Size classification was carried out on plants grown under long day conditions. Images of the flowers from each transformant were acquired using a ZEISS Axio Zoom.V16 equipped with a ZEISS Axiocam 305 color camera. Image analysis to determine vegetative area and flower anatomy was performed using Fiji. Experiments were repeated four times independently, yielding comparable results.

Subcellular localization of FLIPE sensors

Roots of 5–7-day-old seedlings expressing variously targeted FLIPE sensors were imaged using an Olympus IXplore SpinSR confocal microscope equipped with UPLSAPO 60× 1.3 NA silicone immersion oil objective (Olympus, Hamburg, Germany), 50 μm spinning disk, and Photometrics Prime BSI sCMOS camera. A 40-mW coherent OBIS LX 514 nm laser was used to excite YFP using a 445/514/640 nm dichroic and 534/23 nm emission filter for detection. Laser power and acquisition time were adjusted to accommodate differences in brightness among lines.

Additional experiments were performed to validate the localization of the FLIPE^{display} sensor facing the apoplasm.

Subcellular localization assays were adapted from Martinière et al. (2018) and repeated twice, yielding comparable results. Transient expression of the sensors was performed in leaves of 3–4-week-old *Nicotiana benthamiana* plants infiltrated with *A. tumefaciens* strain GV3101 carrying constructs for FLIPE-1m^{display} and FLI^{81}IPE-1μ^{cyt}, as described below. In brief, 3 days past infiltration, protoplasts were obtained by digesting transformed leaves with 1.2% cellulose Onozuka R10 (catalog no. C8001; Duchefa Biochemie), 0.4% macerozyme R10 (catalog no. M8002; Duchefa Biochemie) in 0.4 M mannitol and MES 20 mM (pH 6.5) for 6–8 h at room temperature in the dark by shaking at 1 g. Protoplasts were pelleted at 100 g and rinsed with fresh buffer. Preincubation with 50 μM CHX (catalog no. 66-81-9; Sigma-Aldrich) for 30 min was followed by digestion with proteinase K at 50 μg ml^{-1} and 50 μM CHX. Slides with protoplasts were imaged under a confocal microscope for at least 20 min. Venus fluorescence intensity was quantified using Fiji (Schindelin et al., 2012).

Glutamate supplementation of FLIPE seedlings

Glutamate supplementation experiments were performed by measuring the growth of seedlings transformed with FLIPE constructs on square petri dishes with AM agar medium supplemented with 1% sucrose (catalog no. 57-50-1; Sigma-Aldrich) (as described above) covered with a layer of nylon mesh (Sefar Nitex 03-15/10). Three days after germination, seedlings on the mesh were transferred to an AM agar medium supplemented with 1% sucrose and 0 μM, 25 μM, 100 μM, 250 μM, or 1 mM L-glutamic acid monosodium salt monohydrate (catalog no. 6106-04-3; Sigma-Aldrich). Plants were analyzed in single blinded experiments. After transfer, plates were rotated 90° and plant were grown for 7 days under long day conditions (16 h light, 8 h dark). Seedlings were photographed daily during glutamate treatment and roots were measured using ImageJ (rsb.info.nih.gov/ij/). Experiments were repeated three independent times and yielded comparable results.

Root tip modified pseudo-Schiff–propidium iodide staining

Modified pseudo-Schiff–propidium iodide staining was performed as described by Truernit et al. (2008), on root tips 5 days after germination. Samples were fixed in fixative solution (50% methanol [catalog no. 67-56-1; Sigma-Aldrich] and 10% acetic acid [catalog no. 64-19-7; Sigma-Aldrich]) at 4°C overnight. Root tips were washed with water and incubated in 1% periodic acid at room temperature for 40 min. Then, tissues were rinsed and incubated in Schiff's reagent (catalog no. 3952016; Sigma-Aldrich) with propidium iodide (100 mM sodium metabisulfite and 0.15 N HCl; propidium iodide to a final concentration of 100 μg ml^{-1} freshly

added) until samples were visibly stained. Roots were transferred to chloral hydrate solution (70% chloral hydrate [catalog no. 302-17-0; Sigma-Aldrich], 10% glycerol [catalog no. 56-81-5; Sigma-Aldrich]) and slides were prepared for microscope analysis adding drops of chloral hydrate solution and left covered overnight. The samples were examined with a 40× water immersion objective. Samples stained with propidium iodide were excited with a 561-nm argon laser with emission detection at 566–718 nm.

Total protein extraction and protein gel blot analyses

Plant tissue was freshly harvested from 6- to 7-day-old *A. thaliana rdr6-11* controls or plants expressing FLIPE-600n^{apo}, FLII^{81}PE-1μ^{cyt}, or FLIPE-600n^{dis} constructs and ground to a fine powder in liquid nitrogen. The protein extraction was performed by adding 1 mlg^{-1} fresh weight ice-cold extraction buffer (50 mM Tris-HCl [pH 7.5], 150 mM NaCl, 10% glycerol, 2 mM EDTA, 5 mM DTT, 1% Triton X-100, protease inhibitor mix [1 tablet; Roche, Basel, Switzerland]), followed by vigorous vortexing. The extracts were centrifuged (20 000 ***g***, 30 min, 4°C) and the supernatant was collected. A purified GFP-tagged protein served as control. Protein gel-blotting procedures followed standard protocols. In brief, Laemmli buffer was added to the samples, which were denatured at 95°C for 7 min. Samples were loaded and run on a 4–20% precast polyacrylamide gel (4561094; Bio-Rad, Hercules, CA, USA; 10 μl per sample, except FLIPE-600n^{display}: 20 μl) and subsequently electroblotted on to a PVDF membrane for immunoanalysis. After transfer, membranes were blocked with 3% milk powder and incubated with a GFP antibody from Abcam, Cambridge, UK (catalog no. ab13970, 1:5000 dilution, 4 h) or Roche (catalog no. 11814460001, 1:1000 dilution, overnight). Both antibodies also detect the GFP variant Venus, which is part of the FLIPE sensor. Bound antibodies were visualized using the goat antichicken IgY (H + L) Alexa Fluor 488 (catalog no. A-11039, 1:5000 dilution, 2 h; Thermo Fisher Scientific, Waltham, MA, USA) according to the manufacturer's instructions and α-mouse horseradish peroxidase (catalog no. A-9044, 1:50 000 dilution, 2–3 h; Sigma) as secondary antibodies, respectively. The fluorescence activity of the Alexa Fluor 488 was detected in tiling acquisition mode using the Zeiss Axio Zoom.V16 scope and excitation at 470/40 nm. For detecting the horseradish peroxidase secondary antibody, the ECL SuperSignal™ West Femto (34094; Thermo Fisher Scientific) was used with subsequent visualization on a LAS-4000 Mini bioimager (GE Healthcare Life Sciences, Freiburg, Germany). Images were analyzed with ImageJ (rsb.info.nih.gov/ij/). Contrast and intensities were adjusted separately for the extracted samples and the control to avoid signal saturation in the control.

Quantitative imaging

Quantitative imaging was carried out as described previously (Chaudhuri et al., 2011). In brief, 7-day-old seedlings grown on hydroponic media were mounted on coverslips (24 × 50 mm no. 1.5; VWR) using medical adhesive (stock no. 7730; Hollister) to restrict movement (Deuschle et al., 2006). Chambers used for screening were made with plastic clay (Sculpey, www.sculpey.com) and were variable in size and volume (1–2 ml). For qualitative analyses, the clay chamber was filled with hydroponic medium, perfusion tubing was mounted, and roots were perfused at 3 ml min^{-1}. Ratio imaging was performed on an inverted fluorescence microscope (DM IRE2; Leica, Wetzlar, Germany) with a QuantEM digital camera (Roper, Sarasota, FL, USA) and a ×20 oil objective (HC PL APO ×20/0.7IMM CORR; Leica). Dual emission intensities were recorded simultaneously using a DualView with a dual CFP/YFP-ET filter set (high transmission modified Magnetron sputter-coated filter sets ET470/24m [470 indicates the emission wavelength, 24 indicates bandwidth]; ET535/3; Bellows Falls, VT, USA) and Slidebook software (Intelligent Imaging Innovations Inc., Denver, CO, USA). Data were analyzed with ImageJ (rsb.info.nih.gov/ij/).

ACKNOWLEDGEMENTS

We would like to thank Rüdiger Simon's group for assistance with propidium iodide staining of roots and the Center for Advanced Imaging (CAi) at HHU for help with image acquisition. This research was funded by grants from Deutsche Forschungsgemeinschaft (DFG, German Research Foundation) under Germany´s Excellence Strategy—EXC-2048/1—project ID 390686111 and Deutsche Forschungsgemeinschaft (DFG, German Research Foundation) SFB 1208—Project-ID 267205415 – as well as the Alexander von Humboldt Foundation to WBF. Open access funding enabled and organized by ProjektDEAL.

AUTHOR CONTRIBUTIONS

Conceptualization was done by VCR, MMW, SO, WBF, and TK; methodology was performed by FA, NG, SO, VCR, TK, TD, MT, and MMW; FA, NG, SO, VCR, TK, MM, and MMW performed the investigation; VCR, TK, WBF and MMW wrote the paper; supervision: WBF, TK, MMW.

CONFLICT OF INTEREST

The authors declare that they have no competing interests.

SUPPORTING INFORMATION

Additional Supporting Information may be found in the online version of this article.

Figure S1. Schematic representation of FLIPE and FLII^{81}PE sensor variants.

Figure S2. Fluorescence in *rdr6-11* Arabidopsis seedlings expressing different FLIPE sensors and detailed growth characterization.

Figure S3. *In vitro* saturation curves from FLIPE-40μ, FLIPE-250μ, and FLIPE-500μ sensors.

Figure S4. Phenotypic characterization of additional FLIPE sensor-expressing plants.

Figure S5. Characterization of plants expressing different FLII^{81}PE variants.

Figure S6. Subcellular localization of FLIPE-600n targeting variants in roots.

Figure S7. *In vivo* characterization of FLIPE-10μ^{display} in Arabidopsis roots.

Figure S8. *In vivo* proteinase K digestion assay of protoplasts expressing FLIPE sensors.

Figure S9. Protein gel blot analyses of different plant-expressed FLIPE variants.

Figure S10. Effect of FLIPE-600n^{display} sensor expression on root development.

Figure S11. t-distributed Stochastic Neighbor Embedding (t-SNE) representation of single cell transcriptional profiling from Arabidopsis roots.

OPEN RESEARCH BADGES

This article has earned Open Data and Open Materials badges.

Plasmids generated in this work will be available through Addgene.

DATA AVAILABILITY STATEMENT

Original data are available at: https://osf.io/tmhyx/?view_only=b84de3fee1cb4ed5bc9c8d498fbd0174

REFERENCES

Alfieri, A., Doccula, F.G., Pederzoli, R., Grenzi, M., Bonza, M.C., Luoni, L. et al. (2020) The structural bases for agonist diversity in an Arabidopsis thaliana glutamate receptor-like channel. *Proceedings of the National Academy of Sciences*, **117**, 752–760.

Armbruster, M., Dulla, C.G. & Diamond, J.S. (2020) Effects of fluorescent glutamate indicators on neurotransmitter diffusion and uptake. *eLife*, **9**, e54441.

Barnett, L.M., Hughes, T.E. & Drobizhev, M. (2017) Deciphering the molecular mechanism responsible for GCaMP6m's Ca^{2+}-dependent change in fluorescence. *PLoS One*, **12**, e0170934.

Chaudhuri, B., Hörmann, F. & Frommer, W.B. (2011) Dynamic imaging of glucose flux impedance using FRET sensors in wild-type Arabidopsis plants. *Journal of Experimental Botany*, **62**, 2411–2417.

Chu, L.-C., Offenborn, J.N., Steinhorst, L., Wu, X.N., Xi, L., Li, Z. et al. (2021) Plasma membrane calcineurin B-like calcium-ion sensor proteins function in regulating primary root growth and nitrate uptake by affecting global phosphorylation patterns and microdomain protein distribution. *New Phytologist*, **229**, 2223–2237.

Denyer, T., Ma, X., Klesen, S., Scacchi, E., Nieselt, K. & Timmermans, M.C.P. (2019) Spatiotemporal developmental trajectories in the Arabidopsis root revealed using high-throughput single-cell RNA sequencing. *Developmental Cell*, **48**, 840–852.e5.

Deuschle, K., Chaudhuri, B., Okumoto, S., Lager, I., Lalonde, S. & Frommer, W.B. (2006) Rapid metabolism of glucose detected with FRET glucose nanosensors in epidermal cells and intact roots of Arabidopsis RNA-silencing mutants. *The Plant Cell*, **18**, 2314–2325.

Deuschle, K., Okumoto, S., Fehr, M., Looger, L.L., Kozhukh, L. & Frommer, W.B. (2005) Construction and optimization of a family of genetically encoded metabolite sensors by semirational protein engineering. *Protein Science*, **14**, 2304–2314.

Forde, B.G. & Lea, P.J. (2007) Glutamate in plants: metabolism, regulation, and signalling. *Journal of Experimental Botany*, **58**, 2339–2358.

Frommer, W.B., Davidson, M.W. & Campbell, R.E. (2009) Genetically encoded biosensors based on engineered fluorescent proteins. *Chemical Society Reviews*, **38**, 2833–2841.

Gronnier, J., Crowet, J.-M., Habenstein, B., Nasir, M.N., Bayle, V., Hosy, E. et al. (2017) Structural basis for plant plasma membrane protein dynamics and organization into functional nanodomains. *eLife*, **6**, e26404.

Hajdukiewicz, P., Svab, Z. & Maliga, P. (1994) The small, versatile pPZP family of Agrobacterium binary vectors for plant transformation. *Plant Molecular Biology*, **25**, 989–994.

Hirner, A., Ladwig, F., Stransky, H., Okumoto, S., Keinath, M., Harms, A. et al. (2006) Arabidopsis LHT1 is a high-affinity transporter for cellular amino acid uptake in both root epidermis and leaf mesophyll. *The Plant Cell*, **18**, 1931–1946.

Huang, F., Luo, J., Ning, T., Cao, W., Jin, X., Zhao, H. et al. (2017) Cytosolic and nucleosolic calcium signaling in response to osmotic and salt stresses are independent of each other in roots of Arabidopsis seedlings. *Frontiers in Plant Science*, **8**, 1648.

Kiss, J.Z., Wright, J.B. & Caspar, T. (1996) Gravitropism in roots of intermediate-starch mutants of *Arabidopsis*. *Physiologia Plantarum*, **97**, 237–244.

Li, J., Zhu, S., Song, X., Shen, Y.I., Chen, H., Yu, J. et al. (2006) A rice glutamate receptor-like gene is critical for the division and survival of individual cells in the root apical meristem. *The Plant Cell*, **18**, 340–349.

Mahmoud, S., Gharagozloo, M., Simard, C. & Gris, D. (2019) Astrocytes maintain glutamate homeostasis in the CNS by controlling the balance between glutamate uptake and release. *Cells*, **8**, 184.

Martinière, A., Gibrat, R., Sentenac, H., Dumont, X., Gaillard, I. & Paris, N. (2018) Uncovering pH at both sides of the root plasma membrane interface using noninvasive imaging. *Proceedings of the National Academy of Sciences of the United States of America*, **115**, 6488–6493.

Marvin, J.S., Borghuis, B.G., Tian, L., Cichon, J., Harnett, M.T., Akerboom, J. et al. (2013) An optimized fluorescent probe for visualizing glutamate neurotransmission. *Nature Methods*, **10**, 162–170.

Mousavi, S.A.R., Chauvin, A., Pascaud, F., Kellenberger, S. & Farmer, E.E. (2013) GLUTAMATE RECEPTOR-LIKE genes mediate leaf-to-leaf wound signalling. *Nature*, **500**, 422–426.

Nguyen, C.T., Kurenda, A., Stolz, S., Chételat, A. & Farmer, E.E. (2018) Identification of cell populations necessary for leaf-to-leaf electrical signaling in a wounded plant. *Proceedings of the National Academy of Sciences of the United States of America*, **115**, 10178–10183.

Okumoto, S., Jones, A. & Frommer, W.B. (2012) Quantitative imaging with fluorescent biosensors. *Annual Review of Plant Biology*, **63**, 663–706.

Okumoto, S., Looger, L.L., Micheva, K.D., Reimer, R.J., Smith, S.J. & Frommer, W.B. (2005) Detection of glutamate release from neurons by genetically encoded surface-displayed FRET nanosensors. *Proceedings of the National Academy of Sciences of the United States of America*, **102**, 8740–8745.

Sabetta, W., Vandelle, E., Locato, V., Costa, A., Cimini, S., Moura, A.B. et al. (2019) Genetic buffering of cyclic AMP in *Arabidopsis thaliana* compromises the plant immune response triggered by an avirulent strain of *Pseudomonas syringae* pv. *tomato*. *The Plant Journal*, **98**, 590–606.

Schindelin, J., Arganda-Carreras, I., Frise, E., Kaynig, V., Longair, M., Pietzsch, T. et al. (2012) Fiji: an open-source platform for biological-image analysis. *Nature Methods*, **9**, 676–682.

Singh, S.K. & Chang, I.-F. (2017) Pharmacological studies with specific agonist and antagonist of animal iGluR on root growth in *Arabidopsis thaliana*. In *GABA and Glutamate—new developments in neurotransmission research*: IntechOpen. https://doi.org/10.5772/intechopen.72121

Singh, S.K., Chien, C.-T. & Chang, I.-F. (2016) The Arabidopsis glutamate receptor-like gene GLR3.6 controls root development by repressing the Kip-related protein gene KRP4. *Journal of Experimental Botany*, **67**, 1853–1869.

Toyota, M., Spencer, D., Sawai-Toyota, S., Jiaqi, W., Zhang, T., Koo, A.J. et al. (2018) Glutamate triggers long-distance, calcium-based plant defense signaling. *Science*, **361**, 1112–1115.

Truernit, E., Bauby, H., Dubreucq, B., Grandjean, O., Runions, J., Barthelemy, J. et al. (2008) High-resolution whole-mount imaging of three-dimensional tissue organization and gene expression enables the study of phloem development and structure in Arabidopsis. *The Plant Cell*, **20**, 1494–1503.

Vincill, E.D., Clarin, A.E., Molenda, J.N. & Spalding, E.P. (2013) Interacting glutamate receptor-like proteins in phloem regulate lateral root initiation in Arabidopsis. *The Plant Cell*, **25**, 1304–1313.

Walch-Liu, P., Liu, L.-H., Remans, T., Tester, M. & Forde, B.G. (2006) Evidence that L-glutamate can act as an exogenous signal to modulate root growth and branching in *Arabidopsis thaliana*. *Plant and Cell Physiology*, **47**, 1045–1057.

Wang, X., Yang, G., Shi, M., Hao, D., Wei, Q., Wang, Z. et al. (2019) Disruption of an amino acid transporter LHT1 leads to growth inhibition and low yields in rice. *BMC Plant Biology*, **19**, 268.

Willis, R.C. & Furlong, C.E. (1975) Purification and properties of a periplasmic glutamate-aspartate binding protein from *Escherichia coli* K12 strain W3092. *Journal of Biological Chemistry*, **250**, 2574–2580.